 doi:10.20944/preprints202206.0404.v1

Article

Activated Carbon-added $Li_4Ti_5O_{12}$/Sn Composite Synthesized through Sol-Hydrothermal Method for Anode Active Material in Lithium-ion Battery

Benediktus Ma'dika, Balqis Nabila, and Anne Z. Syahrial*

Department of Metallurgical and Materials Engineering, Faculty of Engineering, Universitas Indonesia,16424 Depok, Jawa Barat, Indonesia
benediktus.madika@alumni.ui.ac.id (B.M.)
* Correspondence: *anne@metal.ui.ac.id; Tel.: +62 812-917-857

Abstract: $Li_4Ti_5O_{12}$ (LTO) exhibits zero-strain behavior, exceptional cycle stability, low cost, and high safety. However, it is still low in electronic and ionic conductivity. Incorporating Sn into LTO materials can increase electronic conductivity and specific capacity. However, Sn still experiences volumetric expansion during the charging/discharging process. Adding activated carbon (AC) into the LTO/Sn composite can help improve the expansion resistance and electronic conductivity. In this work, the AC was first synthesized from charcoals through the carbon activation process and mixed with LTO precursors through the sol-hydrothermal method followed by mixing with Sn through the mechanochemical process to produce LTO@AC/Sn composites. The Sn content was fixed at 15 wt.%, while the AC contents were varied at 1 wt.%, 3 wt.%, and 5 wt.%. The AC specific surface area is increased by more than 100% compared to the non-activated one. The best effects of AC on grain morphology and distribution were found in the LTO/Sn contained 3 wt.% of AC, leading to transfer resistance, ohmic resistance, specific capacity, and coulombic efficiency were found to be 48.1 Ω, 8.5 Ω, 138 $mAhg^{-1}$, and near 100%, respectively. The result suggests that the LTO@AC/Sn could be a favorable anode active material in lithium-ion batteries.

Keywords: activated carbon; lithium-ion batteries; LTO/Sn composite; sol-hydrothermal

1. Introduction

Research on battery technologies for applications in electric vehicles (EVs) has been progressively conducted to alleviate the carbon emission and global warming concern [1]. Li-ion battery (LIB) technologies have commenced the first step toward transportation and domestic energy storage electrification, leading to reduced dependence of our society on fossil fuels[2]. The superior properties of LIBs such as high voltage, high energy and power density, low self-discharge rate, low memory effects, and extended life cycles enable LIBs to meet their potential applications in large-scale energy storage systems and EVs [2,3]. Furthermore, LIBs work based on the intercalation/de-intercalation mechanism in which lithium-ions are either absorbed from the electrolyte solution and inserted into the electrode material (intercalation process) or expelled from the electrode to the electrolyte (de-intercalation process), depending on the direction of the current flow applied[4]. Therefore, lithium does not react with the electrode material, rendering LIBs more stable chemically than other batteries.

Spinel $Li_4Ti_5O_{12}$ (LTO) is an interesting material to be utilized as the active anode material in LIBs owing to its high lithium-ion insertion/de-insertion voltage of 1.55 V versus Li/Li^+, zero-strain nature, excellent cycle stability, stable discharge voltage, high coulombic efficiency, compatibility with the commonly used electrolyte solution, obvious charge/discharge platform, nontoxicity and relatively low-cost[1]. However, LTO still has a low ionic conductivity (3×10^{-10} S cm^{-1} at ambient temperature) attributable to its

 doi:10.20944/preprints202206.0404.v1

poor reversible capacity at high charge/discharge rates, a low electronic conductivity (10^{-6} S cm^{-1} at even 227 ^{0}C), a low lithium-ion diffusion coefficient (1.6×10^{-11} cm^2 s^{-1}) as a result of the initial energy barrier of lithium-ion insertion being very high (over 0.58 eV), and much lower theoretical capacity (about 175 mAh g^{-1}) compared to that of the commercial graphite anode, hindering its broader applications in large-scale energy storage technologies[5,6].

There have been many works conducted to improve the LTO lithium-ion diffusion coefficient and/or electrochemical conductivity. Several of them added Sn to the LTO because Sn possesses a high specific capacity and a high electronic conductivity[5-8]. In this regard, Sn plays its role based on the alloying mechanism with a fully lithiated $Li_{4.4}Sn$ phase that leads to a high specific capacity of 994 mAh g^{-1} and volumetric capacities in the range of 7,216 to 9,786 mAh cm^{-3} [7]. Nevertheless, the continuous uptake and release of lithium ions in the LTO anode containing Sn cause massive volume expansion up to 260 %, and huge stress inside the anode material, making the anode material cracked and pulverized, and thus ultimately breaking the electronic conductive networks around the Sn phase[7].

The addition of carbon to the LTO/Sn material can address the above-mentioned Sn drawbacks. This is because carbon can act as a buffer layer that absorbs internal stresses arising from the Sn expansion and provide conductive networks for charge transfer that enable increased electrical conductivity[8]. In this study, activated carbon (AC) was used on account of its remarkable electrochemical stability and improved specific surface area (SSA) so which is expected to increase the specific capacity larger than that of graphite [9], [10]. Besides, the AC also functions to control the LTO grain growth by homogenizing LTO powders that further enhance the lithium-ion diffusion into the TiO_2 phase, hereafter speeding up the formation of the pristine LTO phase [11]. Still, AC also provides pores that act as paths to supply lithium-ions directly to the LTO phase, allowing rapid lithium-ion transport[12].

We, in this work, synthesized the AC-added LTO/Sn, designated as the LTO@AC/Sn, through the sol-hydrothermal method followed by the mechanochemical process. We used the sol-hydrothermal method because it can produce nano-sized grains with good electrochemical performances [5]. In this typical work, the AC was derived from charcoals and activated by NaOH. To make the LTO@AC/Sn, the AC and LTO precursors (titanium tetra-butoxide ($Ti(OBu)_4$) and LiOH powders) were mixed first through the sol-hydrothermal method to produce an LTO@AC mixture. The mixture of AC, TiO_2, and LiOH had been expected to effectively suppress the formation of the rutile TiO_2 phase [11]. Lastly, the resulting product was then mixed again with Sn powders through the mechanochemical process to produce the desirable LTO@AC/Sn. The Sn content was fixed at 15 wt.% according to the previous work[13] , while the AC contents were varied at 1 wt.%, 3 wt.%, and 5 wt.%. The AC content variations were the variables to make three different LTO@AC/Sn composites.

Several physical characteristics of the prepared LTO@AC/Sn composites were explored by performing X-ray diffraction (XRD), scanning electron microscopy (SEM)-energy dispersive X-Ray spectroscopy (EDS), and Brunauer–Emmett–Teller (BET) method. Meanwhile, the LTO@AC/Sn electrochemical performances were measured by executing cyclic voltammetry (CV), charge-discharge (CD) test, and electrochemical impedance spectroscopy (EIS).

2. Materials and Methods

2. 1 Synthesis of Activated Carbon (AC)

Synthesis of AC referred to a previous work[14] in which the charcoals were ball-milled at 1,800 RPM for 30 minutes to obtain the fine carbon powders followed by heating in a furnace at 500 ^{0}C for 2 hours. To initialize the carbon activation process, the distilled

water was mixed with NaOH pellets and then stirred to render the NaOH pellets homogenous. Then, the carbon activation process was performed by mixing the NaOH pellets and carbon with a ratio of 3:1 correspondingly, for 2 hours at room temperature. The mixture was then dried out in a closed oven at 130 ^{0}C for 24 hours followed by heating in a furnace under the flowing N2 gas at 700 ^{0}C for 1.3 hours. The resulting mixture was washed slowly with 0.1M HCl solution until reaching pHs in the range of 6.5-7 followed by final washing in hot distilled water. The synthesized AC was finally dried at 110 ^{0}C for one day.

2. 2 Synthesis of LTO@AC/Sn Composite

LTO@AC/Sn was synthesized through the sol-hydrothermal method followed by the mechanochemical process. First, we prepared the primary solution consisting of titanium tetra-butoxide ($Ti(OBu)_4$), ethanol (pH 3), AC (with contents of 1 wt. %, 3 wt.%, and 5 wt.%), while the secondary solution consisted of ethanol (pH 3) and distilled water. Then, the primary solution was titrated by the secondary solution until the desirable sol-gel phase was formed. The result was dried for 5 days under the ambient atmosphere until the crystals of TiO_2-AC xerogel were formed. Afterward, the crystals were crushed into fine powders and then calcined at 300 ^{0}C for 2 hours under the flowing pure O_2 gas.

Meanwhile, the hydrothermal process was performed at 135 ^{0}C for 15 hours in an autoclave with its bottom filled with distilled water. The product was then ball-milled with LiOH powders at 900 RPM for 15 minutes followed by calcining at 750 ^{0}C for 3 hours to obtain the LTO@AC powders. Finally, the obtained powders were ball-milled with Sn powders (the content of 15 wt.%) at 900 RPM for 15 minutes to produce the intended LTO@AC/Sn composites. The LTO@AC/Sn variations were designated as LTO@1%AC/15%Sn, LTO@3%AC/15%Sn, and LTO@5%AC/15% Sn corresponding to the amount of AC content added.

2. 3 Physical Characterization

The SSA of AC was determined by performing the BET method under the liquid N_2 gas at 77.3K (Quantachrome NovaWin). The SEM-EDS characterization (VEGA 3 TESCAN, voltage of 15.0 kV, high vacuum) was performed to investigate the morphologies and elemental composition of AC, and LTO@AC/Sn after being mixed with a binder and an additive conductive. XRD characterization was performed to determine the phase present in the LTO@AC/Sn composite materials.

2. 4 Electrochemical Performance Measurement

To investigate the electrochemical performances of the LTO@AC/Sn composites, the synthesized LTO@AC/Sn as the anode active material, acetylene black as the additive conductive, and polyvinylidene fluoride (PVDF) as the binder, with a ratio of 8:1:1 respectively, were first mixed homogenously in the dimethylacetamide (DMAC) solution to produce a slurry. The doctor blade technique was employed to coat the slurry onto the Cu foil as the current collector. The result was dried up at 80 ^{0}C for 1.5 hours to produce the anode materials. They were then cut into the size of the CR2032 cell. LIB half-cells were constructed using LiPF6 as the electrolyte, the prepared anode material as the working electrode, lithium metal foil as the opposing electrode, and polypropylene as the separator. The assembly of the cell was done in an Ar gas-filled glovebox. Finally, the electrochemical characteristics of each half-cell were measured by several techniques. EIS was used to reveal the resistivity value, while the CV test was done to know the cell voltage, specific capacity, and electrochemical stability and reversibility. CD was done to obtain the charging/discharging capacity and capability performances from low to high current rates (C-rates).

 doi:10.20944/preprints202206.0404.v1

3. Results and Discussion

3.1 Activated Carbon (AC)

The AC physisorption isotherm curve obtained from the BET characterization is displayed in **Figure 1**. The shape of the curve is concave downward to the p/p^0 axis and has a steep uptake at the very low p/p^0. This mode indicates that the curve falls under Type I(b) isotherm which is sometimes exhibited by microporous solids, such as activated carbon, whose pore size distributions range from wider micropores to narrow mesopores [15].

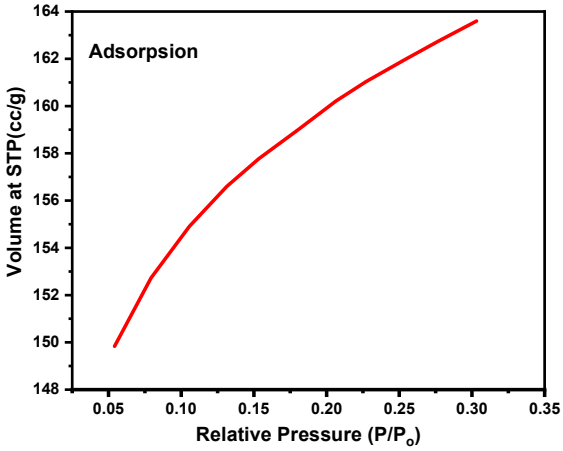

Figure 1. AC Physisorption isotherm curve.

The SSA of the AC was found to be 490.007 $m^2\ g^{-1}$ which is much greater than that of the same charcoal-derived carbon without an activation process (224.847 $m^2\ g^{-1}$). The increased SSA of AC was the outcome of the NaOH activating agent that reacted with active surfaces of the charcoal-derived carbon, thus: i) releasing CO, CO_2, and H_2 gases that further created micropores on the AC surface; ii) enabling the alkali metal (Na) to intercalate into the AC structure and form micropores on the AC structures [16]. The high SSA of AC provides plentiful active sites for lithium-ion storage, while its porous structures shorten the diffusion length of lithium-ions in the overall bulk electrode [10].

Figure 2 displays the SEM characterization of AC. Some of the AC particles were agglomerated (**Figure 2a**). In this figure, formed pores only look like small dots, and therefore, we needed much larger SEM magnification to investigate them more clearly as displayed in **Figure 2b** where we observe pores exist as marked in red circles. The size of the pores was about 2 μm which is still classified as macropores [15]. Even though the synthesized AC is macroporous, it has a much larger SSA (more than 100%) compared to that of the same charcoal-derived carbon without an activation process as stated previously.

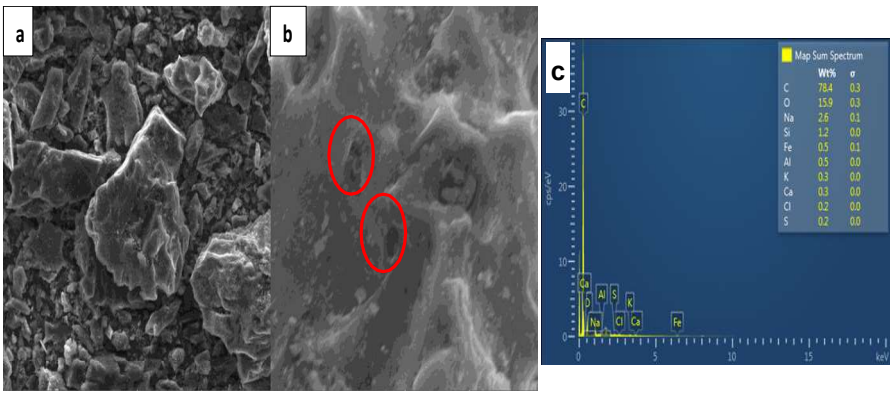

Figure 2.SEM images of AC with magnification: (a) 1,000X ,and (b) 5,000X; and (c) EDX map sum spectrum of elements present in AC.

Figure 2c presents the elemental composition contained in the AC. Carbon content is found to be 78.4%, while the rest percentage is for other elements. There was no prior characterization performed to obtain the information on the elemental contents before the activation process was started, so we could not make a comparison of the element contents before and after the activation process. Cl in the AC was expected to originate from HCl solution, while Na likely came from the NaOH. Other elements are suspected of coming from the raw material and chemically uncontrolled environment during the synthesizing process.

3.2 Physical Characteristics of LTO@AC/Sn Composites

XRD characterizations shown in **Figure 3** inform us that there are several phases formed in each of the LTO@AC/Sn composites: $Li_4Ti_5O_{12}$ (JCPDS NO. 49-0207) [17], rutile-TiO_2 (JCPDS NO. 01-1292) [18], anatase-TiO_2 (JCPDS NO. 21-1272) [17], Li_2TiO_3 (JCPDS NO. 08-0249)[19],Sn (JCPDS No. 01-0926)[20], and carbon[21]. The formation of rutile-TiO_2, anatase-TiO_2, and Li_2TiO_3 indicates that the LTO was not completely formed during the sol-hydrothermal process. The rutile-TiO_2 and anatase-TiO_2 might be originated from the non-optimal calcination process performed at 750 ^{0}C for 3 hours. It was because some of the metastable phases underwent thermal decomposition into rutile-TiO_2, anatase-TiO_2, LTO, or other forms at high calcining temperatures[5], [22]. According to the previous work, the mixture of AC in an appropriate content with TiO_2 and LiOH could effectively suppress the formation of the rutile-TiO_2 phase at high temperatures [11]. Therefore, we can see from the figure that the peaks of the rutile-TiO_2 are shorter in LTO@3%AC/15%Sn and LTO@5%AC/15% compared to those in LTO@1%AC/15%Sn. This corresponds to the AC contents in LTO@3%AC/15%Sn and LTO@5%AC/15% are larger than that in LTO@1%AC/15%Sn. Meanwhile, Li_2TiO_3 is sometimes formed together with $Li_4Ti_5O_{12}$ during the non-optimal sol-hydrothermal process [5]and/or also when the amount of lithium compound is excessive[23]. Carbon peaks are identified emerging at two significant diffraction peaks at nearby 24° and 43° [21]. On the other hand, the highest Sn peak in each LTO@AC/Sn composite appeared at the same 2θ value (30.6^0) and nearly the same intensity. This is because the content of Sn powders added was the same for all the LTO@AC/Sn composites.

 doi:10.20944/preprints202206.0404.v1

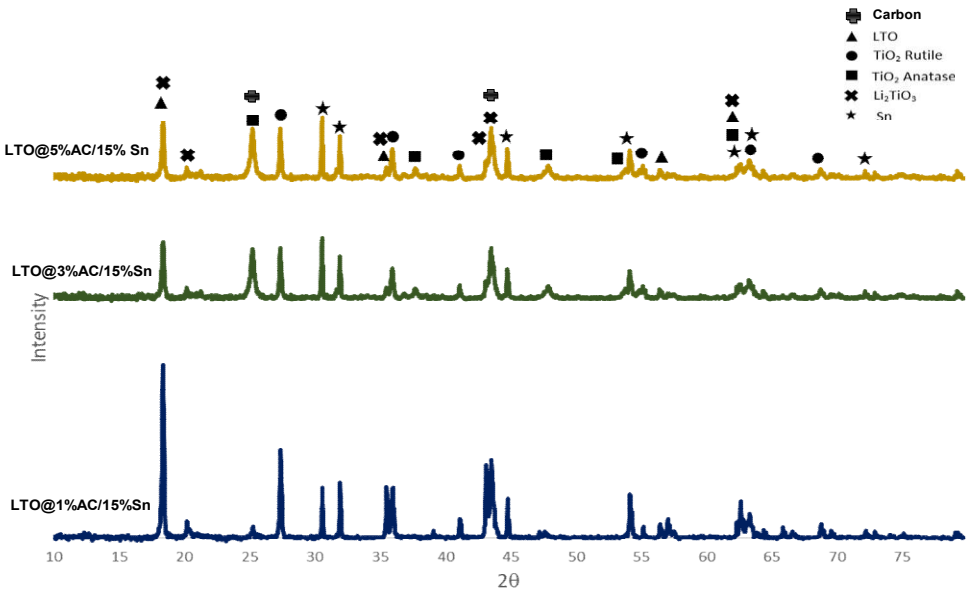

Figure 3.XRD characterization of LTO@1%AC/15%Sn, LTO@3%AC/15%Sn, and LTO@5%AC/15%.

SEM characterizations were performed after mixing each of the LTO@AC/Sn composites with the additive conductive, and the binder. The results are shown in **Figure 4** where each LTO@AC/Sn displays different grain morphologies and distributions. LTO@1%AC/15%Sn exhibits some LTO/Sn grains that were agglomerated to form bulk particles in some places (red circles in **Figure 4a**.) and some were distributed throughout the anode material in closer proximity to each other. This might be the effect of the smaller AC content added in comparison with the LTO/Sn content so that the AC particles were separated and then isolated in the LTO/Sn matrix [24]. On the contrary, LTO@3%AC/15%Sn displays smaller grains distributed throughout the anode material, and the grains were in closer proximity to each other as shown in **Figure 4b**. This indicates that the AC content of the LTO@3%AC/15%Sn composite is the most favorable to control the LTO/Sn grain growth into smaller sizes in this work. The suitable amount of AC content enables a higher rate transformation of Li_2TiO_3-to-$Li_4Ti_5O_{12}$ while the conversion of the anatase-to-rutile TiO_2 becomes negligible[13].

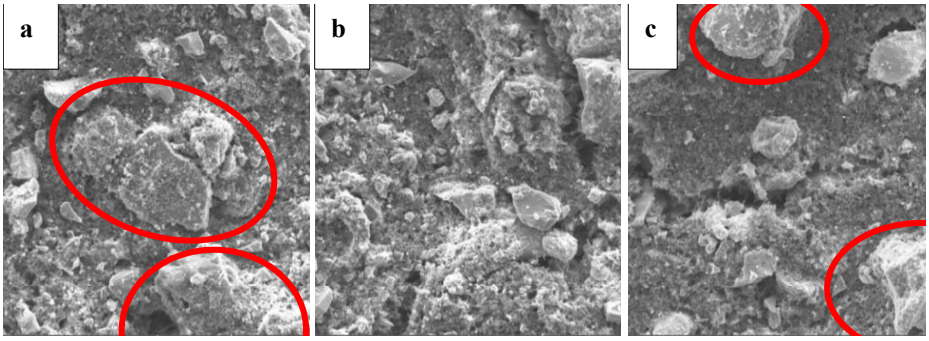

Figure 4. SEM images (magnification of 1,000X) of (a) LTO@1%AC/15%Sn, (b) LTO@3%AC/15%Sn, and (c) LTO@5%AC/15%.

On the other side, LTO@5%AC/15% displays that the LTO/Sn phase was less visible than other anode phases. Only a few of the LTO/Sn grains are visible yet agglomerated

 doi:10.20944/preprints202206.0404.v1

forming bulk particles (red circles as shown in **Figure 4c**.). This is because of the cumulative effect of the carbon from the AC and the additive conductive forming highly interconnected carbon networks in the LTO/Sn composite matrix, making the phase incline to agglomerate into particles in the micro-meter range [24]. Excessive AC content might also have hampered interfacial reaction at LiOH/anatase-TiO_2 interface, leading to the sluggish formation of metastable Li_2TiO_3 layer and increased formation rate of anatase-to-rutile TiO_2 [11]. To conclude, LTO@3%AC/15%Sn has the best grain morphology and distribution in this work.

The EDS map sum spectrums of elements that existed in the LTO@AC/Sn composites are shown in **Figure 5**. Elements detected in each composite are C, F, Ti, O, Sn, Cl, and Cu. However, Li could not be detected because its generated X-ray signal is low and the probability of absorption high, leading to emitted intensity being small [25]. C has the largest content in each composite, and it is expected to come from the AC and additive conductive, while F was likely to originate from the PVDF. LTO@5%AC/15%Sn has the highest carbon content followed by LTO@3%AC/15%Sn, and finally LTO@1%AC/15%. The presence of Ti and O indicates the existence of LTO, rutile-TiO_2, anatase-TiO_2, and Li_2TiO_3 phases. Cl is suspected to come from the HCl, while Cu is predicted to come from the copper foil.

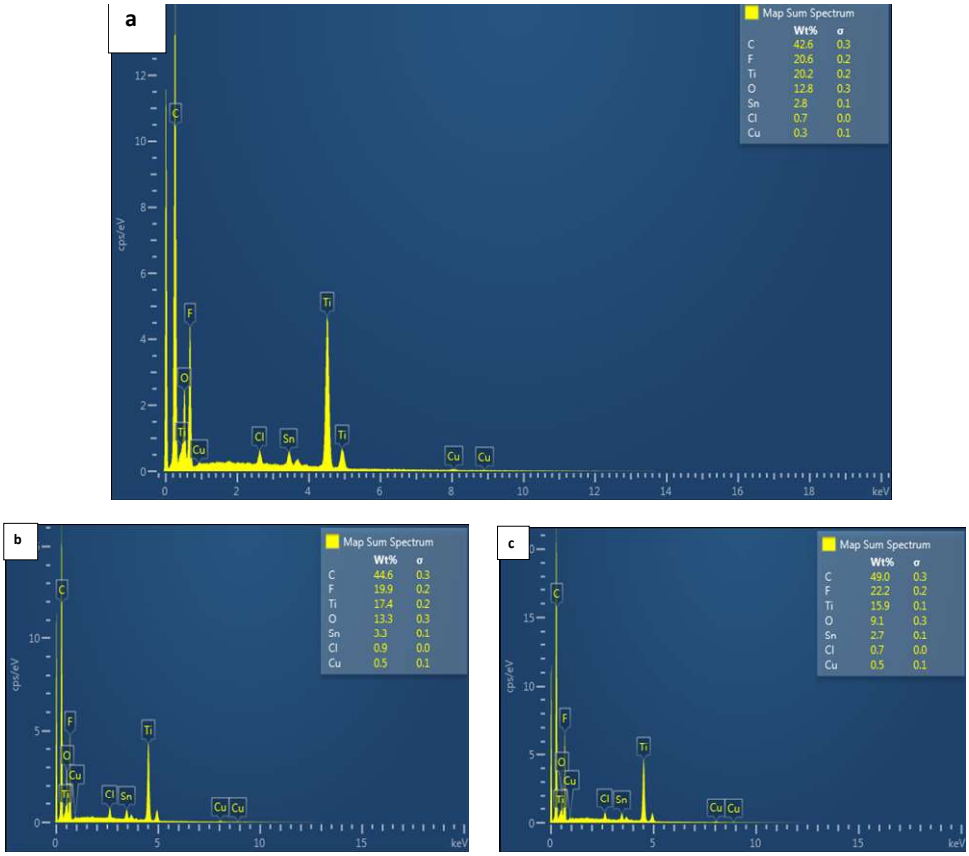

Figure 5.EDS mapping of (a) LTO@1%AC/15%Sn, (b) LTO@3%AC/15%Sn, and (c) LTO@5%AC/15%.

3.3 Electrochemical Performance of LTO@AC/Sn Composites

Figure 6 shows the cyclic voltammograms of the LTO@AC/Sn composites. From these graphs, we can investigate the reversibility phase reaction characteristics during

Preprints (www.preprints.org) | NOT PEER-REVIEWED | Posted: 29 June 2022 doi:10.20944/preprints202206.0404.v1

lithium-ion intercalation and deintercalation processes. Three main peaks emerge at both anodic and cathodic curves. To find out the working potential (E^0) of the phases, we, then, averaged the anodic potential peak ($E_{p,a}$) and cathodic potential peak ($E_{p,c}$) with the equation below [26].

$$E^0 = \frac{E_{p,a}+E_{p,c}}{2} \quad (3.1)$$

The averaged potential peaks (as marked with red lines in the graphs) of one couple of anodic and cathodic potential of LTO@1%AC/15%Sn, LTO@3%AC/15%Sn, and LTO@5%AC/15% are found to be 1.56, 1.52, 1.49 V, respectively. These potentials are expected to belong to the LTO working potential because they are very close to the LTO working potential (~1.5V) [5]. Other peaks that emerge in the graphs at 2.07 V belong to the TiO_2 phase [27]. In addition, the peaks that exist from 0.6 to 0.8 V indicate the working potential of Sn [28]

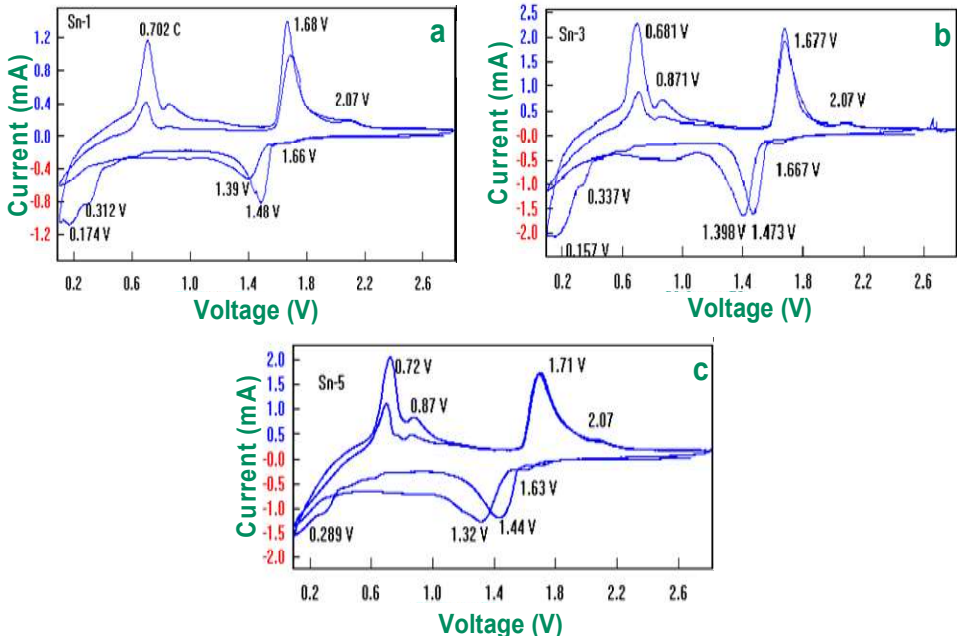

Figure 6. Cyclic voltammogram: (a) LTO@1%AC/15%Sn, (b) LTO@3%AC/15%Sn, and (c) LTO@5%AC/15%.

Still, we can see that LTO@1%AC/15%Sn (**Figure 6a**) and LTO@3%AC/15%Sn **Figure 6b**) have sharper and higher peaks compared to those in LTO@5%AC/15% (**Figure 6c**), indicating that LTO@1%AC/15%Sn and LTO@3%AC/15%Sn have better fast charging/discharging characteristics due to the faster lithium-ion diffusion rate than those of LTO@5%AC/15% [11]. However, LTO@3%AC/15%Sn still has better reversibility than LTO@1%AC/15%Sn because it has more superimposed curves or more stable cycling. This superior intercalation/deintercalation characteristics of LTO@3%AC/15%Sn corresponds to its smaller and evenly distributed grains throughout the anode material. Small-sized grains increase the contact area between the active material particles themselves and the active material particles and the electrolyte solution and shorten the diffusion length of lithium ions, enhancing the kinetics of the lithiation/de-lithiation process [29]. Therefore, cyclability can be maintained during several scans. Another interesting thing to be investigated in **Figure 6** is the shape of the cyclic voltammograms. LTO@1%AC/15%Sn and LTO@3%AC/15%Sn almost have the same shape (battery mode), while the

 doi:10.20944/preprints202206.0404.v1

LTO@5%AC/15% tends to have a rectangular shape (capacitive electrode mode). This indicates that the high content of AC added into the LTO@AC/Sn composite tends to make the cell to be capacitive. This phenomenon has also been observed in the work of Mathias Widmaier et.al (2017) [24]. Peak broadening and shifting in LTO@3%AC/15%Sn are the consequences of the deterioration of kinetics of the lithiation/de-lithiation process [24] .

Figure 7 presents the specific capacities of LTO@1%AC/15%Sn, LTO@3%AC/15%Sn, and LTO@5%AC/15% whose values are 125, 138, and 156.9 mAh g^{-1}, correspondingly. These data provide us insight that the increased AC content in the LTO@AC/Sn composite can enhance the specific capacity. The highest specific capacity value obtained is 156.9 mAh g^{-1} which belongs to LTO@5%AC/15%. This is because LTO@5%AC/15% contains the largest AC content providing large sites for lithium-ion storage [30].

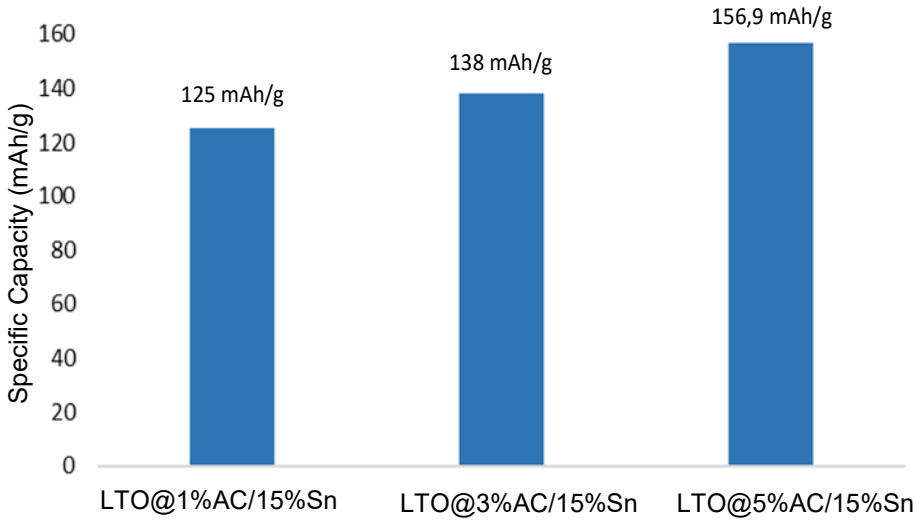

Figure 7. Specific capacity of LTO@1%AC/15%Sn, LTO@3%AC/15%Sn, and LTO@5%AC/15%.

However, the specific capacity of each LTO@AC/Sn composite as shown in **Figure 7** is still lower than that of pristine LTO (175 mAh g^{-1} at ~1.55 V vs. Li/Li^+) [6] and much lower than that of pristine Sn (994 mAh g^{-1}) [7]. Sn did not increase the specific capacity significantly as expected before. This might be due to the Sn content being larger than should be so that it reduced the surface area of the composite down to a lower value than that of the original LTO [31], leading to poorer electrochemical performance. Still, the presence of unwanted impurities such as anatase-TiO_2 and rutile-TiO_2 might be also the cause. TiO_2 has low electronic and ionic conductivities that limit its specific capacity [6], while the anatase-TiO_2 possesses poor capacity retention attributable to its grains tending to be agglomerated and fractured during the lithium-ion intercalation, causing the lithium-ion path damage and formation of lithium-ion transport barriers[32]. These lead to drastically reduced specific capacities. Li_2TiO_3 is not expected to present undesired effects because it can form an LTO/Li_2TiO_3 composite which can strengthen the structural stability of the host materials and provide fast lithium-ion conduction characteristics [23].

The charge/discharge capacity and rate capability measurements of LTO@AC/Sn composites were performed at C-rates of 0.5, 0.2,1,2,4,8,12, 15, and 20 C from 0.0 to 2.5 V. The corresponding charge/discharge capacity and rate capability curves are shown in **Figure 8**. LTO@1%AC/15%Sn and LTO@3%AC/15%Sn exhibit better charge/discharge capacity at high rates up to 20 C, indicating that they have better high-rate capability than LTO@5%AC/15% as displayed in **Figure 8a**. Still, the curves of LTO@1%AC/15%Sn (**Figure 8b**) and LTO@3%AC/15%Sn (**Figure 8c**) exhibit the initial charge capacities are almost

 doi:10.20944/preprints202206.0404.v1

the same as the maximum discharge capacities achieved at each C-rate, signifying that these two composites have good electrochemical reversibility.

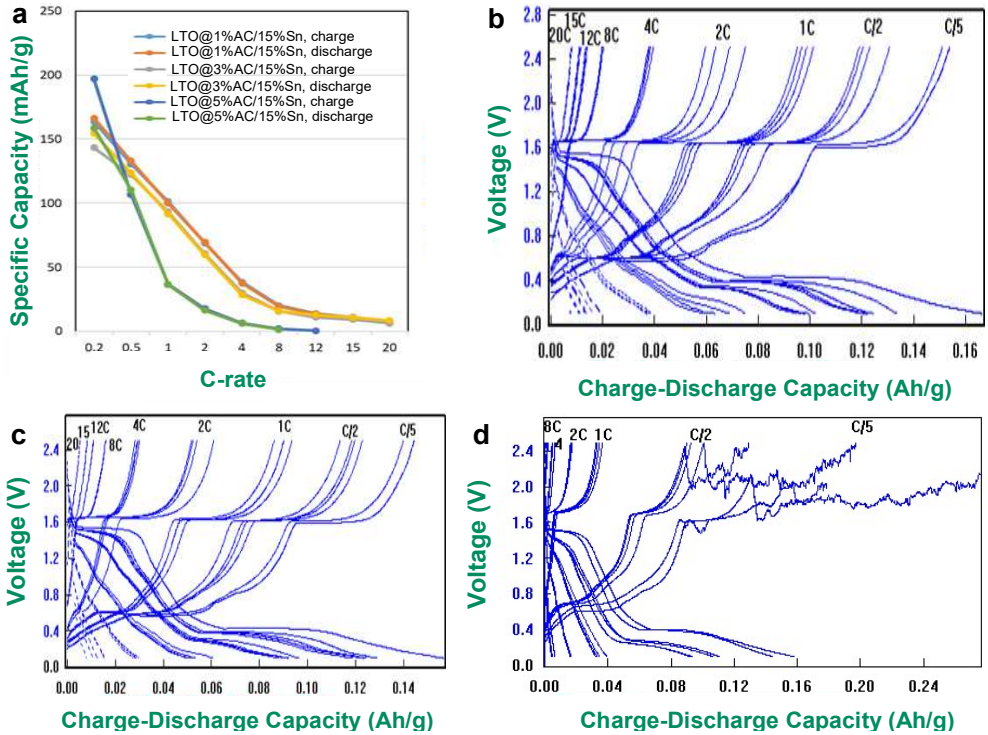

Figure 8. (a) specific capacity versus C-rate for all composite anodes, charge/discharge performance at various C-rate for (b) LTO@1%AC/15%Sn, (c) LTO@3%AC/15%Sn, and (d) LTO@5%AC/15%.

The better cycle performances of LTO@3%AC/15%Sn correspond to their LTO/Sn grains were well-distributed throughout the anode material and close to each other as explained previously. This can, particularly at high rates, facilitate better mass transfer capability [10] and faster lithium-ion mobility due to the shorter overall distance traveled by lithium-ions, leading to a higher overall specific capacity of the material [31].

In contrast, LTO-5%C/15%Sn has a significant difference in the initial charge capacity and discharge capacity achieved at high C-rates (**Figure 8**a), showing that this material is poor in terms of electrochemical reversibility. **Figure 8d**, furthermore, displays that LTO@5%AC/15% exhibits a significantly larger initial charge capacity compared to the discharge capacity, revealing a large irreversible capacity. The high first cycle insertion capacity is attributable to the high AC content which has high SSA providing abundant pores for lithium-ion storage, while the low first cycle de-insertion capacity might be caused by the solid electrolyte interface (SEI) formation at the first discharge process, the decomposition of the carbonate-based electrolyte, and irretrievable lithium-ions intercalating into deeper sites of AC material [30]. Furthermore, higher content of AC in LTO@5%AC/15% leads to structural collapse of the AC material at high rates when the lithium-ions are released from the material during the cycling [30]. In addition, excessive AC content in LTO@5%AC/15% might have hindered or even blocked interfacial reaction at LiOH/anatase-TiO_2 interface causing the slow formation of the Li_2TiO_3 layer and increasing the formation rate of anatase-to-rutile TiO_2. The presence of the rutile-TiO_2 in LTO@5%AC/15% might further deteriorate the charge/discharge capacity and capability of LTO@5%AC/15% at high C-rates. Therefore, the charge/discharge capacity and capability of LTO@5%AC/15% at high rates are the worst in this work.

 doi:10.20944/preprints202206.0404.v1

Still, in **Figure 8**, the specific capacity of each composite at higher current rates (>10 C) suffered significant declines, and the curves exhibit bad cycling stability when the charge/discharge current rates are higher than 10 C. This phenomenon is attributed to characteristics of the LTO/TiO[33] composite[33]. The charge/discharge plateaus close to the voltage of 1.5 V (versus Li/Li^+) also became much shorter and even vanished with the increased C-rates (>10 C) cycled from 0 to 2.5 V due to the electrochemical polarization of the LTO/TiO_2

To obtain more electrochemical performances of the LTO@AC/Sn composite anodes, we calculated the coulombic efficiency (CE) using the equation below [34] and the result is presented in Figure 9.

$$\mathrm{CE} = \frac{\text{Discharge capacity}}{\text{Charge Capacity}} \times 100\% \qquad (3.2)$$

CE is usually used to estimate the cycling life of LIB because it reflects the loss of lithium-ions during each charge/discharge cycling[34]. LTO@1%AC/15%Sn and LTO@3%AC/15%Sn exhibit efficiency values that are close to 100% at each current rate from 0.2 to 20 C.This means that almost no side reactions are occurring in LTO@1%AC/15%Sn and LTO@3%AC/15%Sn during each charge/discharge cycling, leading to good cycle capability and electrochemical reversibility. However, LTO@5%AC/15% at 0.2 C and 8 C exhibits CE values that are quite far from 100%. In addition, LTO@5%AC/15% lost its capability to be charged and discharged at 12 C, 15 C, and 20 C, so that there are no efficiency values presented in these rates. These poor performances of LTO@5%AC/15% are suspected attributing to the formation of not electrochemically active by-products and structural damage, leading to poor cycle capability and lithiation/de-lithiation irreversibility [34].

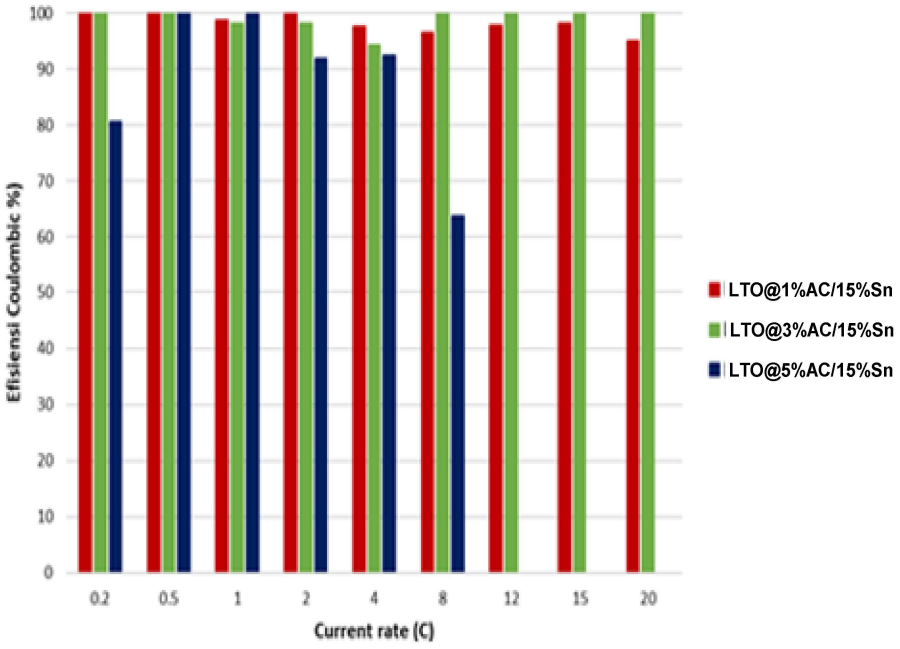

Figure 9. Coulombic efficiency values of LTOC/Sn composite anodes.

EIS measurements were further performed to study the electrochemical reaction kinetics of the lithiation/de-lithiation into/ from the LTO@AC/Sn composite material. **Figure 10** presents the Nyquist plot obtained during the EIS measurement of each of the composites, and their corresponding resistivity values are presented in **Table 1**. We can observe

 doi:10.20944/preprints202206.0404.v1

that inside the high-frequency portion, each curve has a semicircle while inside the low-frequency portion has an upright line with a slope of 45^0. However, the line is not too significant in the case of LTO@1%AC/15%Sn and LTO@5%AC/15%. The intercept at the real axis (Z_{real}), the radius of the semicircle, and the upright line correspond to the ohmic resistance (R_s), charge transfer resistance (R_{ct}), and Warburg impedance (Z_W), in that order. R_s is formed due to the electronic conductivity of the separator, electrolyte, and anodes, while ZW is stemmed from the diffusion of lithium-ions in the active materials[33].

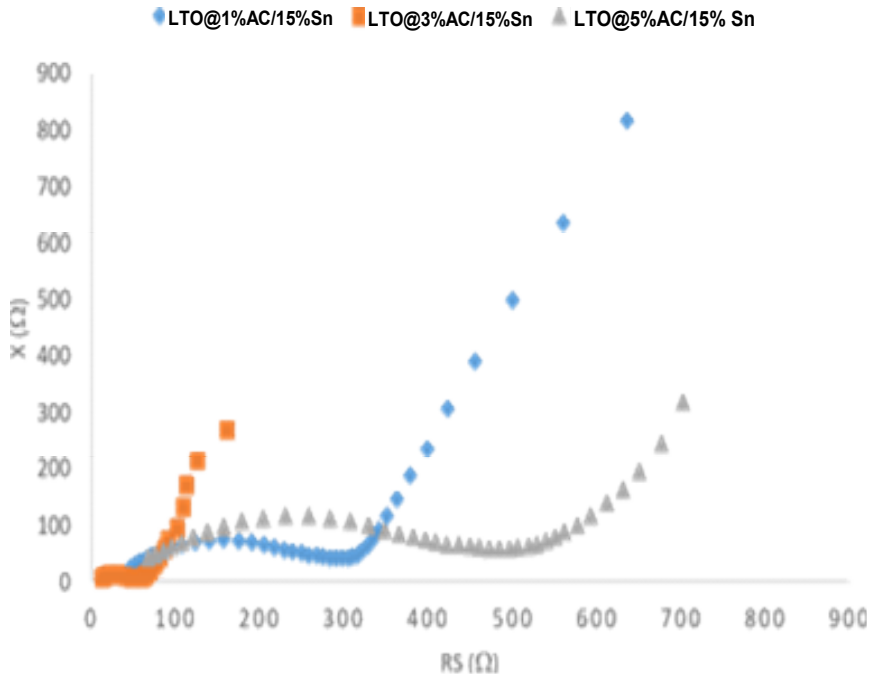

Figure 10. Nyquist plot of each LTO@AC/Sn composite anodes.

Table 1.Resistance values of each composite anodes.

LTO@/AC/Sn Composite	R_s(Ω)	R_{ct} (Ω)
LTO@1%AC/15%Sn	46.92	257.19
LTO@3%AC/15%Sn	8.50	48.10
LTO@1%AC/15%Sn	67.53	528.34

From **Figure 10**, we can also observe that LTO@3%AC/15%Sn has the most suppressed and smallest semicircle followed by the LTO@1%AC/15%Sn and then LTO@5%AC/15%. The smallest semicircle means the lowest R_{ct} and the highest electrochemical conductivity. Therefore, LTO@3%AC/15%Sn has the lowest R_{ct} value (48.1Ω) as shown in **Table 1**. LTO@3%AC/15%Sn possesses this behavior because it has small and well-distributed LTO/Sn grains containing conductive Sn across the anode material plus the suitable AC content serving as the networks for charge transfer. Small and well-distributed grains are close to each other and thus shorten the path of charge transfer, leading

 doi:10.20944/preprints202206.0404.v1

to reduced R_{ct}. On the contrary, LTO@1%AC/15%Sn has agglomerated LTO/Sn grains, while LTO@5%AC/15% contains too excessive carbon and some agglomerated LTO/Sn grains that are not well-distributed in the anode materials. Agglomerated and not well-distributed grains tend to separate with each other, and hence prolong the charge transfer, leading to increased R_{ct}. In addition, the excessive amount of AC in LTO@5%AC/15% increases resistivity attributable to the porous microstructure of carbon and therefore enhances the overall bulk resistance[31].

Still, we can see from **Table 1** that LTO@3%AC/15%Sn has the smallest R_s followed by LTO@1%AC/15%Sn and then LTO@5%AC/15%Sn. Smallest R_s means the smallest resistance of the ionic transfer from the electrolyte to the electrode material and vice versa. The reduced LTO@3%AC/15%Sn solution resistance is again attributable to its well-distributed and small LTO/Sn grains and the enhanced SSA of AC, enhancing the contact area between the LTO@AC/Sn composite material and the electrolyte solution.

4. Conclusions

Synthesis of AC from charcoals was successfully achieved through the NaOH activation process resulting in an increased specific surface area by more than 100% compared to that of the same carbon-derived charcoals without the activation process. The sol-hydrothermal and mechanochemical methods were successfully conducted to synthesize the desirable LTO/AC/Sn composite material, but it still contained TiO_2 (anatase and rutile) and Li_2TiO_3. AC was observed to control the morphologies and distribution of the LTO/Sn composite grains in the anode material. The AC with the content of 3%. wt. (LTO@3%AC/15%Sn) is the best because it prevents the LTO/Sn composite grains from getting agglomerated and enabled the grains to grow into smaller sizes. Therefore, LTO@3%AC/15%Sn has the best overall electrochemical performance as the anode active material. Its charge transfer resistance, specific capacity, and coulombic efficiency were found to be 48.1 Ω, 138 $mAhg^{-1}$, and near 100%, correspondingly. This result suggests that LTO@3%AC/15%Sn could be a promising candidate as an active material for LIB anode. However, the expectation of the composite to have both the enhanced specific capacity and reduced resistivity at the same time due to the presence of Sn and AC was not met. This is because the above-mentioned impurities are present, and they are suspected to stem from the non-optimal calcination temperature and duration. For further research, we recommend using optimal time and temperature for the calcination process, and the activation AC step should be more strictly controlled to get high-quality AC.

Author Contributions: Conceptualization,B.N.; methodology,B.N; formal analysis B.M.; investigation, B.N.; resources, B.N.; writing—original draft preparation, B.M; writing—review and editing, B.M; visualization,B.M; supervision, A.Z.S.; project administration A.Z.S.; funding acquisition,A.Z.S. All authors have read and agreed to the published version of the manuscript.

Funding: This research was funded by the Ministry of Education and Culture, the Republic of Indonesia, grant number 008/E4.1/AK.04.PRN/2021 under the PRN-BOPTN Project.

Data Availability Statement: Not applicable.

Acknowledgments: The authors would like to express their gratitude for financial support from the Ministry of Education and Culture, the Republic of Indonesia under the PRN-BOPTN Project, with contract number: 008/E4.1/AK.04.PRN/2021.

Conflicts of Interest: The authors declare no conflict of interest. The funders had no role in the design of the study; in the collection, analyses, or interpretation of data; in the writing of the manuscript; or in the decision to publish the results.

References

[1] H. Yan, D. Zhang, Qilu, X. Duo, and X. Sheng, "A review of spinel lithium titanate ($Li_4Ti_5O_{12}$) as electrode material for advanced energy storage devices," *Ceramics International*, vol. 47, no. 5. Elsevier, pp. 5870–5895, Mar. 01, 2021. doi: 10.1016/j.ceramint.2020.10.241.

[2] Marinaro M, Bresser D, Beyer E, Faguy P, Hosoi K, Li H, Sakovica J, Amine K, Wohlfahrt-Mehrens M, Passerini S, "Bringing forward the development of battery cells for automotive applications: Perspective of R&D activities in China, Japan, the EU and the USA," *Journal of Power Sources*, vol. 459, no. 1, pp. 1–8, Jul. 2020, doi: 10.1016/j.jpowsour.2020.228073.

[3] G. dos Reis, C. Strange, M. Yadav, and S. Li, "Lithium-ion battery data and where to find it," *Energy and AI*, vol. 5. Elsevier, p. 100081, Sep. 01, 2021. doi: 10.1016/j.egyai.2021.100081.

[4] G. L. Plett, "Battery Boot Camp," *Battery management systems. Volume 1 : battery modeling*, pp. 1–28, 2015.

[5] T. F. Yi, T. T. Wei, Y. Li, Y. B. He, and Z. B. Wang, "Efforts on enhancing the Li-ion diffusion coefficient and electronic conductivity of titanate-based anode materials for advanced Li-ion batteries," *Energy Storage Materials*, vol. 26, pp. 165–197, Apr. 2020, doi: 10.1016/J.ENSM.2019.12.042.

[6] S. Wang, Y. Yang, Y. Dong, Z. Zhang, and Z. Tang, "Recent progress in Ti-based nanocomposite anodes for lithium ion batteries," *Journal of Advanced Ceramics 2019 8:1*, vol. 8, no. 1, pp. 1–18, Mar. 2019, doi: 10.1007/S40145-018-0292-2.

[7] W. Li, X. Sun, and Y. Yu, "Si-, Ge-, Sn-Based Anode Materials for Lithium-Ion Batteries: From Structure Design to Electrochemical Performance," *Small Methods*, vol. 1, no. 3. pp. 22–30, 2017. doi: 10.1002/smtd.201600037.

[8] T. Zeng, X. Hu, P. Ji, Q. Peng, B. Shang, and S. Gong, "General synthesis of nano-M embedded $Li_4Ti_5O_{12}$/C composites (M = Sn, Sb and Bi) with high capacity and good cycle stability," *Electrochimica Acta*, vol. 217, pp. 299–309, Nov. 2016, doi: 10.1016/j.electacta.2016.09.075.

[9] Jiang Y, Li J, Jiang Z, Shi M, Sheng R, Liu Z, Zhang S, Cao Y, Wei T, Fan Z, "Large-surface-area activated carbon with high density by electrostatic densification for supercapacitor electrodes," *Carbon N Y*, vol. 175, pp. 281–288, Apr. 2021, doi: 10.1016/j.carbon.2021.01.016.

[10] X. Yang, C. Wei, and G. Zhang, "Activated carbon aerogels with developed mesoporosity as high-rate anodes in lithium-ion batteries," *Journal of Materials Science*, vol. 51, no. 11, pp. 5565–5571, Jun. 2016, doi: 10.1007/s10853-016-9861-3.

[11] A. Subhan, F. Oemry, S. N. Khusna, and E. Hastuti, "Effects of activated carbon treatment on $Li_4Ti_5O_{12}$ anode material synthesis for lithium-ion batteries," *Ionics 2018 25:3*, vol. 25, no. 3, pp. 1025–1034, Jun. 2018, doi: 10.1007/S11581-018-2633-0.

[12] Zhao E, Qin C, Jung HR, Berdichevsky G, Nese A, Marder S, Yushin G, "Lithium Titanate Confined in Carbon Nanopores for Asymmetric Supercapacitors," *ACS Nano*, vol. 10, no. 4, pp. 3977–3984, Apr. 2016, doi: 10.1021/acsnano.6b00479.

[13] Syahrial AZ, Aldy F, Priyono B, Subhan A "Enchanced electrochemical performances of $Li_4Ti_5O_{12}$/Sn composites anode via sol-hydrothermal method for lithium ion batteries," *IOP Conference Series: Earth and Environmental Science*, vol. 105, no. 1, p. 012114, Jan. 2018, doi: 10.1088/1755-1315/105/1/012114.

[14] Cazetta AL, Vargas AMM, Nogami EM, Kunita MH, Guilherme MR, Martins AC, Silva TL, Moraes JCG, Almeida VC, "NaOH-activated carbon of high surface area produced from coconut shell: Kinetics and equilibrium studies from the methylene blue adsorption," *Chemical Engineering Journal*, vol. 174, no. 1, pp. 117–125, Oct. 2011, doi: 10.1016/j.cej.2011.08.058.

[15] Thommes M, Kaneko K, Neimark A V., Olivier JP, Rodriguez-Reinoso F, Rouquerol J, Sing KSW, "Physisorption of gases, with special reference to the evaluation of surface area and pore size distribution (IUPAC Technical Report)," *Pure and Applied Chemistry*, vol. 87, no. 9–10, pp. 1051–1069, Oct. 2015, doi: 10.1515/pac-2014-1117.

[16] Z. Heidarinejad, M. H. Dehghani, M. Heidari, G. Javedan, I. Ali, and M. Sillanpää, "Methods for preparation and activation of activated carbon: a review," *Environmental Chemistry Letters 2020 18:2*, vol. 18, no. 2, pp. 393–415, Jan. 2020, doi: 10.1007/S10311-019-00955-0.

[17] Yang L, Li HZ, Liu J, Lu Y, Li S, Min J, Yan N, Men Z, Lei M, "Effects of TiO_2 phase on the performance of $Li_4Ti_5O_{12}$ anode for lithium-ion batteries," *Journal of Alloys and Compounds*, vol. 689, pp. 812–819, Dec. 2016, doi: 10.1016/J.JALLCOM.2016.08.059.

[18] K. I. Ozoemena and S. Chen, "Nanostructure Science and Technology Nanomaterials in Advanced Batteries and Supercapacitors," pp. 1–576, 2016, doi: 10.1007/978-3-319-26082-2.

[19] L. Shen, C. Yuan, H. Luo, X. Zhang, K. Xu, and Y. Xia, "Facile synthesis of hierarchically porous $Li_4Ti_5O_{12}$ microspheres for high rate lithium ion batteries," *Journal of Materials Chemistry*, vol. 20, no. 33, pp. 6998–7004, Aug. 2010, doi: 10.1039/C0JM00348D.

[20] N. Lin, J. Zhou, Y. Han, K. Zhang, Y. Zhu, and Y. Qian, "Chemical synthesis of porous hierarchical Ge-Sn binary composites using metathesis reaction for rechargeable Li-ion batteries," *Chemical Communications*, vol. 51, no. 96, pp. 17156–17159, Nov. 2015, doi: 10.1039/c5cc06178d.

[21] Y. Li, L. Mu, Y. S. Hu, H. Li, L. Chen, and X. Huang, "Pitch-derived amorphous carbon as high performance anode for sodium-ion batteries," *Energy Storage Materials*, vol. 2, pp. 139–145, Jan. 2016, doi: 10.1016/J.ENSM.2015.10.003.

[22] El-Deen SS, Hashem AM, Abdel Ghany AE, Indris S, Ehrenberg H, Mauger A, Julien CM, "Anatase TiO_2 nanoparticles for lithium-ion batteries," *Ionics*, vol. 24, no. 10, pp. 2925–2934, Oct. 2018, doi: 10.1007/s11581-017-2425-y.

[23] Li S, Guo J, Ma Q, Yang Y, Dong X, Yang M, Yu W, Wang J, Liu G, "Electrospun $Li_4Ti_5O_{12}/Li_2TiO_3$ composite nanofibers for enhanced high-rate lithium ion batteries," *Journal of Solid State Electrochemistry*, vol. 21, no. 10, pp. 2779–2790, Oct. 2017, doi: 10.1007/s10008-017-3596-1.

[24] Widmaier M, Jäckel N, Zeiger M, Abuzarli M, Engel C, Bommer L, Presser V, "Influence of carbon distribution on the electrochemical performance and stability of lithium titanate based energy storage devices," *Electrochimica Acta*, vol. 247, pp. 1006–1018, Sep. 2017, doi: 10.1016/J.ELECTACTA.2017.07.073.

[25] Hovington P, Timoshevskii V, Burgess S, Demers H, Statham P, Gauvin R, Zaghib K,"Can we detect Li K X-ray in lithium compounds using energy dispersive spectroscopy?," *Scanning*, vol. 38, no. 6, pp. 571–578, Nov. 2016, doi: 10.1002/sca.21302.

[26] E. M. Espinoza, J. A. Clark, J. Soliman, J. B. Derr, M. Morales, and V. I. Vullev, "Practical Aspects of Cyclic Voltammetry: How to Estimate Reduction Potentials When Irreversibility Prevails," *Journal of The Electrochemical Society*, vol. 166, no. 5, pp. H3175–H3187, Jan. 2019, doi: 10.1149/2.0241905jes.

[27] Jin J, Huang SZ, Liu J, Li Y, Chen LH, Yu Y, Wang HE, Grey CP, Su BL, "Phases Hybriding and Hierarchical Structuring of Mesoporous TiO_2 Nanowire Bundles for High-Rate and High-Capacity Lithium Batteries," *Advanced Science*, vol. 2, no. 7, p. 1500070, Jul. 2015, doi: 10.1002/advs.201500070.

[28] T. Zeng, X. Hu, P. Ji, B. Shang, and Q. Peng, "Promotional role of Li4Ti5O12 as Li^+ conductor and structural stabilizer on Sn@C anode cyclability," *Journal of Alloys and Compounds*, vol. 712, pp. 311–319, Jul. 2017, doi: 10.1016/j.jallcom.2017.03.364.

[29] Kim T, Choi W, Shin HC, Choi JY, Kim JM, Park MS, Yoon WS, "Applications of voltammetry in lithium ion battery research," *Journal of Electrochemical Science and Technology*, vol. 11, no. 1, pp. 14–25, Feb. 2020, doi: 10.33961/JECST.2019.00619.

[30] K. Yu, J. Li, H. Qi, and C. Liang, "High-capacity activated carbon anode material for lithium-ion batteries prepared from rice husk by a facile method," *Diamond and Related Materials*, vol. 86, pp. 139–145, Jun. 2018, doi: 10.1016/J.DIAMOND.2018.04.019.

[31] B. Priyono, A. Z. Syahrial, M. R. Nugraha, D. Sepala, Faizah, and A. Subhan, "Optimizing the performance of microcomposites $Li_4Ti_5O_{12}$/Sn with Sn and $Li_4Ti_5O_{12}$/Sn@C anode and activated carbon content variables for lithium-ion batteries," *International Journal of Technology*, vol. 10, no. 5, pp. 1010–1023, 2019, doi: 10.14716/IJTECH.V10I5.2563.

[32] L. Gao, X. Li, H. Hu, G. Li, H. Liu, and Y. Yu, "TiO_2 mesoporous microspheres with nanorod structure: Facile synthesis and superior electrochemical performance," *Electrochimica Acta*, vol. 120, pp. 231–239, Feb. 2014, doi: 10.1016/J.ELECTACTA.2013.12.020.

[33] M. Ding, H. Liu, X. Zhao, L. Pang, L. Deng, and M. Li, "Composite with TiO_2 and extension of discharge voltage range for capacity enhancement of a Li4Ti5O12 battery," *RSC Advances*, vol. 7, no. 69, pp. 43894–43904, Sep. 2017, doi: 10.1039/C7RA07390A.

[34] Xiao J, Li Q, Bi Y, Cai M, Dunn B, Glossmann T, Liu J, Osaka T, Sugiura R, Wu B, Yang J, Zhang JG, Whittingham MS, "Understanding and applying coulombic efficiency in lithium metal batteries," *Nature Energy*, vol. 5, no. 8, pp. 561–568, Aug. 2020, doi: 10.1038/s41560-020-0648-z.